
DISPERSAL-INDUCED GROWTH IN A TIME-PERIODIC ENVIRONMENT

Guy Katriel

Department of Applied Mathematics, ORT Braude College,
Karmiel, Israel

July 17, 2022

ABSTRACT

Dispersal-induced growth (DIG) occurs when two populations with time-varying growth rates, each of which, when isolated, would become extinct, are able to persist and grow exponentially when dispersal among the two populations is present. This work provides a mathematical exploration of this surprising phenomenon, in the context of a deterministic model with periodic variation of growth rates, and characterizes the factors which are important in generating the DIG effect, and the corresponding conditions on the parameters involved.

1 Introduction

Exploring how the dispersal of organisms interacts with environmental heterogeneity, both spatial and temporal, to determine population growth, is a central theme in ecological theory, with important implications for environmental management and conservation (Baguette et al. [2012], Cousens et al. [2008], Hanski and Gaggiotti [2004], Lewis et al. [2016]). Many plant and animal populations inhabit separate patches of varying size and quality, which are inter-connected by dispersal. A patch is called a *source* if it can sustain a population, and a *sink* if it is of such low quality that a population would not persist on it, if isolated. A basic insight of source-sink theory is that populations in sinks may be sustained, and even exhibit positive growth rates, as a result of immigration from source patches (Dias [1996], Kavecki [2004], Pulliam [1988]). A more surprising phenomenon is that of Dispersal-induced Growth (DIG), whereby it is possible for populations in a set of patches, with dispersal among them, to persist and grow *despite* the fact that *all* these patches are sinks. This counter-intuitive effect was first explicitly discussed, in different frameworks, in Jansen and Yoshimura [1998], Roy et al. [2005]. Jansen and Yoshimura [1998] used a simplified ‘well-mixing’ model with stochastic environment, and occurrence of the DIG effect was derived. Roy et al. [2005], who used the term ‘inflationary effect’ for what we here call dispersal-induced growth, modelled direct dispersal among patches, with stochastic growth rates which are temporally *positively autocorrelated*, and the possibility of the DIG effect was derived by heuristic arguments and demonstrated by extensive numerical simulations. Matthews and Gonzalez [2007] experimentally confirmed the DIG phenomenon in a laboratory system using *Paramecium aurelia*. See also Cheong et al. [2019], Williams and Hastings [2011] for surveys and discussions of ‘paradoxical’ effects in population biology, in which coupling of losing strategies can lead to persistence and growth.

In the continuous-time deterministic context, the DIG phenomenon was discussed and numerically demonstrated by Klausmeier [2008], using a simple two-patch model leading to a pair of ordinary differential equations, with periodic growth rates - see equations (1),(2) below. The present work is devoted to the mathematical analysis of this model. Periodically varying growth rates can either be thought of as a proxy for auto-correlated environmental fluctuations as assumed in the stochastic model of Roy et al. [2005], or they can model seasonal variations in the quality of patches, another ubiquitous ecological mechanism (White and Hastings [2020]). The DIG phenomenon is manifested when, despite the fact that the time-averaged growth rate in each patch is negative, which would lead to extinction in each patch if it were isolated, dispersal among the two patches allows both populations to persist and grow (see figure 1 below). Such persistence may be desirable in the context of species conservation, or undesirable, as in the case of invasive species or pathogens. In the recent work of Kortessis et al. [2020] the same model is obtained as a linearization of an SIR epidemic model, which is used to numerically demonstrate that epidemic control through non-pharmaceutical

interventions may be hampered by the fact that control measures are applied in a non-synchronized manner in different regions which are inter-connected by flows of infective individuals, leading to persistence of a pathogen that would have been eradicated if movement between the two regions had been curtailed, or if the control measures had been synchronized among the regions.

A better understanding of the DIG phenomenon, beyond numerical simulations, requires mathematical analysis of relevant models. For stochastically varying growth, several researchers have obtained analytical results regarding the DIG effect. In the special case of ‘well-mixed’ systems in which dispersing individuals join a common pool from which they disperse to all patches, a simple and elegant analytical treatment is available (Bascompte et al. [2002], Jansen and Yoshimura [1998], Metz et al. [1983]). The case of direct and limited dispersal among patches is considerably more difficult. Morita and Yoshimura [2012] analyze a discrete-time model, showing that the ratio of populations in the two patches converges to a stationary distribution characterized by a Perron-Frobenius equation which can be solved numerically, and in terms of which the total growth rate of the populations can be computed. Evans et al. [2013] analyze a continuous-time stochastic model, obtaining an explicit expression for the stationary distribution in the two-patch case, from which the population growth rate can be calculated, and providing explicit conditions for the occurrence of dispersal-induced growth. In the above-mentioned analytical works, it is assumed that there is no auto-correlation in the environmental variation. Schreiber [2010] obtains an analytical approximation for the population growth rate for the case of many patches in a discrete-time model including auto-correlation of the time-dependent growth rates, which shows that positive autocorrelation enhances the total population growth rate and thus the possibility of DIG, while spatial correlation among patches reduces this effect, in agreement with the numerical findings of Roy et al. [2005].

In the context of time-periodic, rather than stochastic, environmental variation, Bansaye and Lambert [2013] analyze discrete-time models, in which the environment varies periodically among a finite set of states, including a treatment of demographic stochasticity, and conditions for occurrence of DIG are given. It appears that to date there has been no study providing mathematical understanding of the DIG effect in the continuous-time deterministic context, and the conditions under which it does and does not arise. The aim of this work is to perform such an analysis, and to prove that, under appropriate conditions, the DIG phenomenon *must* occur.

We show that occurrence of the DIG effect depends on an appropriate balance of *three* factors:

- (i) Difference in the time-dependence of the growth rates in the two populations: the DIG effect *cannot* occur when the time-dependent growth rates are identical or sufficiently similar.
- (ii) Frequency of the variation in growth rates: this frequency must be sufficiently *small* for DIG to occur.
- (iii) Rate of dispersal: for DIG to occur, dispersal must be neither too weak nor too strong. This was also the case in the stochastic simulations reported in Roy et al. [2005], and the analytical results in Schreiber [2010]. Thus, dispersal, is a ‘double-edged sword’ (Abbott [2011], Hudson and Cattadori [1999]) - its positive effect on population growth is suppressed if its level is too high.

The precise formulations of our results are given in section 2.

Since the differential equations involved, though simple, are not explicitly solvable, our analysis requires some indirect methods for analyzing the behavior of their solutions. We first derive a single nonlinear differential equation for the ratio of the populations in the two patches, and show that the growth rates of the two populations can be expressed using an integral involving the solution of this single equation (section 3). We then analyze the solution for the single equation in two asymptotic regimes for the frequency of oscillations in the growth rate - the low and high frequency limits (sections 4,5, respectively). The approximations obtained allow us to prove that, under appropriate conditions on the periodic profiles of the growth rates and on the dispersal rate, the DIG effect occurs for sufficiently low frequency, and does *not* occur for sufficiently high frequencies, as well as for sufficiently high dispersal rates.

Our results will explain central features of the observations made using numerical simulations, and in particular show that DIG is a robust phenomenon occurring for general periodic growth-rate profiles, as long as the parameters involved are in appropriate ranges. They also characterize several key properties of the region in the parameter space for which DIG occurs. However, there are also several properties of this region, as obtained numerically, which our analytical results do not capture, so that there is room for further mathematical investigations. Some open questions for further research will be presented in the Discussion.

Throughout the paper we present results of numerical simulations and computations, which illustrate the analytical results obtained.

2 The main results

2.1 The model

We consider populations of sizes $x_1(t), x_2(t)$, inhabiting two patches, and subject to time-periodic local growth rates $r_1(\omega t), r_2(\omega t)$, where it is assumed that $r_1(\theta), r_2(\theta)$ are 2π -periodic functions, so that $r_1(\omega t), r_2(\omega t)$ are periodic with period $T = \frac{2\pi}{\omega}$. We also assume dispersal among the two patches at rate $m \geq 0$, leading to the differential equations.

$$x'_1 = r_1(\omega t)x_1 + m(x_2 - x_1), \quad (1)$$

$$x'_2 = r_2(\omega t)x_2 + m(x_1 - x_2). \quad (2)$$

The model studied is linear, as it does not take into account density-dependent effects. However, the study of this system is also directly relevant to the understanding of more elaborate models including nonlinearity, since persistence of populations in such models depends on the behavior of the system obtained by linearization around the trivial equilibrium $(x_1, x_2) = (0, 0)$, which brings us back to the (1),(2), so our results entail the occurrence of the DIG effect in more ‘realistic’ models.

It is easy to show (see section 3) that any solution of (1),(2) with $x_1(0) > 0, x_2(0) > 0$ satisfies $x_1(t) > 0, x_2(t) > 0$ for all $t > 0$.

Given a function $x : [0, \infty) \rightarrow (0, \infty)$ we will denote its growth rate (Lyapunov exponent) by

$$\lambda[x] = \lim_{t \rightarrow \infty} \frac{1}{t} \ln(x(t)),$$

provided this limit exists. Note that $\lambda[x] > 0$ corresponds to exponential growth, while $\lambda[x] < 0$ corresponds to exponential decay - leading to extinction. Therefore our investigation focuses on the quantities $\lambda[x_1], \lambda[x_2]$. In the absence of dispersal ($m = 0$) the population in each patch would evolve independently, and the differential equations are easily solved to yield

$$x_i(t) = x_i(0)e^{\int_0^t r_i(\omega \tau) d\tau}, \quad i = 1, 2, \quad (3)$$

leading to

$$\lambda[x_i] = \lim_{t \rightarrow \infty} \frac{1}{t} \int_0^t r_i(\omega \tau) d\tau = \bar{r}_i,$$

where

$$\bar{r}_i = \frac{1}{2\pi} \int_0^{2\pi} r_i(\theta) d\theta, \quad i = 1, 2.$$

\bar{r}_1, \bar{r}_2 are therefore the *local* average growth rates in each of the patches. Patch i is called a *source* if $\bar{r}_i > 0$ and a *sink* if $\bar{r}_i < 0$.

The study of growth rates $\lambda[x_i]$ when the patches are coupled through dispersal ($m > 0$) is more difficult than in the uncoupled case, since the equations (1), (2) cannot be solved in closed form. It will be shown (Lemma 3) that the growth rates of the two components, $\lambda[x_1], \lambda[x_2]$, are equal, and moreover they do not depend on the initial condition. We will therefore denote the growth rate $\lambda[x_1] = \lambda[x_2]$ corresponding to the system (1),(2) by $\Lambda = \Lambda(m, \omega)$.

We will say that *dispersal-induced growth* (DIG) occurs if both patches are sinks ($\bar{r}_1 < 0, \bar{r}_2 < 0$), but $\Lambda(m, \omega) > 0$. This means that each of the populations would become extinct if isolated, but dispersal, at an appropriate rate, induces exponential growth in both populations.

In the special case in which growth rates are constant in time, $r_1(\theta) = \bar{r}_1, r_2(\theta) = \bar{r}_2$, the system (1),(2) is easily solved, and the growth rate Λ is the dominant eigenvalue of the matrix

$$M = \begin{pmatrix} \bar{r}_1 - m & m \\ m & \bar{r}_2 - m \end{pmatrix}, \quad (4)$$

so that

$$\Lambda = \frac{1}{2} \left[\bar{r}_1 + \bar{r}_2 + \sqrt{(\bar{r}_1 - \bar{r}_2)^2 + 4m^2} - 2m \right] \leq \frac{1}{2} \left[\bar{r}_1 + \bar{r}_2 + \sqrt{(\bar{r}_1 - \bar{r}_2)^2} \right] = \max(\bar{r}_1, \bar{r}_2), \quad (5)$$

and in particular $\Lambda < 0$ whenever $\bar{r}_1 < 0, \bar{r}_2 < 0$. Thus the DIG phenomenon *cannot* occur when growth rates are constant.

Studying the growth or decay of the solutions of the system (1),(2) can be formulated as a question of *Floquet Theory* (Hale [2009], Klausmeier [2008]). Any system of linear differential equations with periodic coefficients has associated

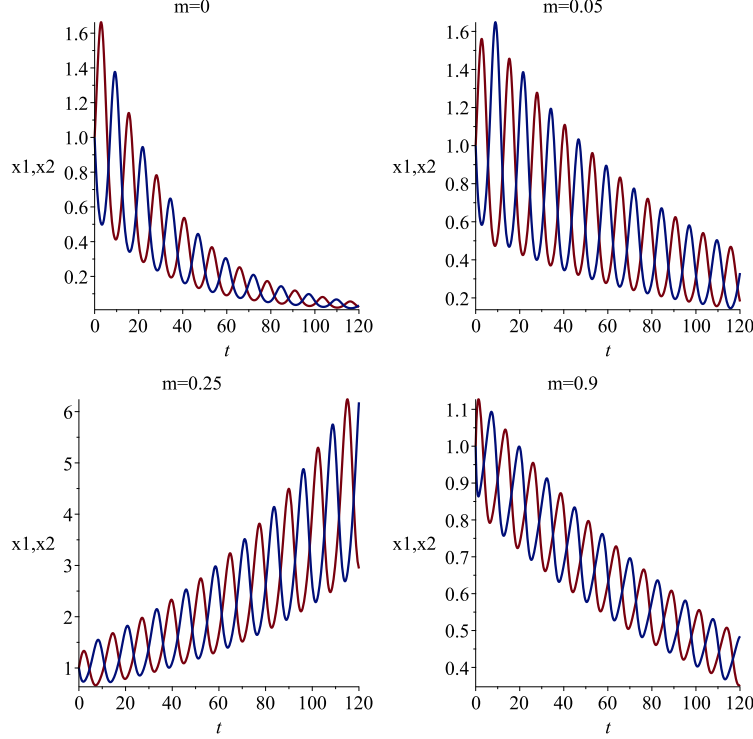


Figure 1: Solutions of (1),(2), with $r_1(\omega t) = -0.03 + 0.3 \cos(\omega t)$, $r_2(\omega t) = r_1(\omega t - \pi)$, with $\omega = 0.5$, for different values of the dispersal rate m .

Floquet exponents, and indeed, in the notation used here, the value Λ is precisely the maximal Floquet exponent - whose sign determines the growth or decay of the solutions. However, in contrast to time-independent (autonomous) systems, studying the Floquet exponents of periodic systems analytically is quite challenging, and our aim is to perform such a study for the particular system of interest here. We obtain explicit expressions for the limiting value of $\Lambda(m, \omega)$ in two cases: $\omega \rightarrow 0$ (low frequency) and $\omega \rightarrow \infty$ (high frequency), and these allow us to study the conditions under which dispersal-induced growth occurs.

2.2 Some numerical results

A numerical demonstration of the DIG effect is shown in figure 1, for a pair of periodic growth-rate profiles with $\bar{r}_1 < 0, \bar{r}_2 < 0$. In the absence of dispersal ($m = 0$), as well as for sufficiently weak dispersal ($m = 0.05$), both populations decay, while in the presence of stronger dispersal ($m = 0.25$) both populations grow - the DIG phenomenon. For yet stronger dispersal ($m = 0.9$) the populations once again decay.

In figure 2, we display a numerically-generated plot of the (m, ω) parameter-plane, for the same periodic growth profiles as in figure 1 - the way in which this figure is generated is explained in Section 3. The green region is the set of parameter values for which $\Lambda(m, \omega) > 0$, that is for which DIG occurs. The lines are level curves of the function $\Lambda(m, \omega)$. As we see in the figure, there exists a finite value $m^* > 0$ such that, if the dispersal rate satisfies $m \in (0, m^*)$, DIG occurs when the frequency ω of environmental variation is sufficiently small, $0 < \omega < \omega_{crit}(m)$, and does not occur if $\omega > \omega_{crit}(m)$, or if $m \geq m^*$.

Defining $\omega^* = \max_{m \in [0, m^*]} \omega_{crit}(m)$, we see that if we fix a frequency $\omega \in (0, \omega^*)$ then DIG will occur for an intermediate range of values of m - neither too weak nor too strong. If $\omega > \omega^*$ DIG will not occur for any dispersal rate. The bottom part of figure 2 shows the growth rate Λ as a function of the dispersal rate m , for three values of the frequency, using the same profiles $r_1(\theta), r_2(\theta)$. Positive values of Λ , corresponding to DIG, occur for intermediate values of m .

A central aim of this work is to obtain a mathematical understanding of the above-noted features, that is to analytically derive some of the key features seen in Figure 2, thus proving that they are generic.

2.3 The Sink-Sink case

We present our main results characterizing the behavior of the two-patch system in the case where both patches are sinks ($\bar{r}_1, \bar{r}_2 < 0$), and then discuss the implications for characterizing the conditions for DIG.

Theorem 1 (Sink-Sink case). *Assume $r_1(\theta), r_2(\theta)$ are continuously differentiable 2π -periodic functions, with $\bar{r}_1 < 0$ and $\bar{r}_2 < 0$. Define*

$$\chi = \frac{1}{2\pi} \int_0^{2\pi} \max(r_1(\theta), r_2(\theta)) d\theta. \quad (6)$$

Then:

(I) If $\chi < 0$ then $\Lambda(m, \omega) < 0$ (decay) for all $m > 0, \omega > 0$.

(II) If $\chi > 0$ then:

A. (Low frequency). The equation

$$\frac{1}{2\pi} \int_0^{2\pi} \sqrt{[r_1(\theta) - r_2(\theta)]^2 + 4m^2} d\theta = 2m - (\bar{r}_1 + \bar{r}_2) \quad (7)$$

has a unique solution $m = m^* > 0$, and we have:

- If $m \in (0, m^*)$ then for any $\omega > 0$ sufficiently small (depending on m), we have $\Lambda(m, \omega) > 0$ (growth).
- If $m > m^*$ then for any $\omega > 0$ sufficiently small (depending on m) we have $\Lambda(m, \omega) < 0$ (decay).

B. For sufficiently high ω (depending on m) we have $\Lambda(m, \omega) < 0$ (decay).

The proof of part (I) of Theorem 1 is given in section 3 (see Lemma 5). Parts (II) A,B of the theorem will be proved in sections 4,5, respectively.

We now discuss the insights that this theorem gives into the DIG effect. This can be compared with the observations regarding the numerical results given in 2.2 above.

(1) **The period growth profiles:** The condition $\chi > 0$, where χ is given by (6) is necessary for DIG to occur. χ can be interpreted as the time-average of the larger of the two local growth rates at each point in time. This condition entails in particular that:

- (i) At least one of the local growth rates must be positive at *some* times. However it is possible for one of the local growth rates to be negative at *all* times, and indeed it is even possible for one of the local growth rates to be negative *and* constant (time-independent) - see figure 3 (left) for such an example.
- (ii) There are some parts of the period during which $r_1(\theta) > r_2(\theta)$, and some for which $r_2(\theta) > r_1(\theta)$. Indeed, if $r_1(\theta) > r_2(\theta)$ for all θ , then we have $\chi = \bar{r}_1 < 0$.
- (iii) The local growth rates r_1, r_2 cannot be too similar (in particular they cannot be identical). Indeed, if $\max_\theta |r_1(\theta) - r_2(\theta)| \leq \epsilon$ then, for $i = 1, 2$,

$$\chi = \frac{1}{2\pi} \int_0^{2\pi} \max(r_1(\theta), r_2(\theta)) d\theta \leq \frac{1}{2\pi} \int_0^{2\pi} \max(r_i(\theta), r_i(\theta) + \epsilon) d\theta = \frac{1}{2\pi} \int_0^{2\pi} (r_i(\theta) + \epsilon) d\theta = \bar{r}_i + \epsilon.$$

Thus, if $\epsilon < \max(|\bar{r}_1|, |\bar{r}_2|)$ then $\chi < 0$. We therefore conclude that if

$$\max_\theta |r_1(\theta) - r_2(\theta)| < \max(|\bar{r}_1|, |\bar{r}_2|),$$

then DIG *cannot* occur. Note, however, that it is possible to have $\chi > 0$ even when r_1, r_2 are phase-synchronized, so that DIG can occur even if the same seasonal effect acts in both patches, as long as the strength of this effect is different in the two patches - see Figure 3 (right) for an example.

(2) **Rate of dispersal.** Assuming that $\chi > 0$, part (II),A of Theorem 1 implies that when $m \in (0, m^*)$ DIG will occur for ω sufficiently small. Thus a dispersal rate which is too large ($m > m^*$) will prevent the DIG effect from occurring, but an arbitrarily small dispersal rate can induce DIG *provided* that the frequency ω is sufficiently small. The qualification in the previous sentence is essential: if we fix $\omega > 0$, then it is easy to see that for sufficiently small m , the DIG effect cannot occur: indeed for $m = 0$ the system decouples into two one-dimensional systems with Floquet

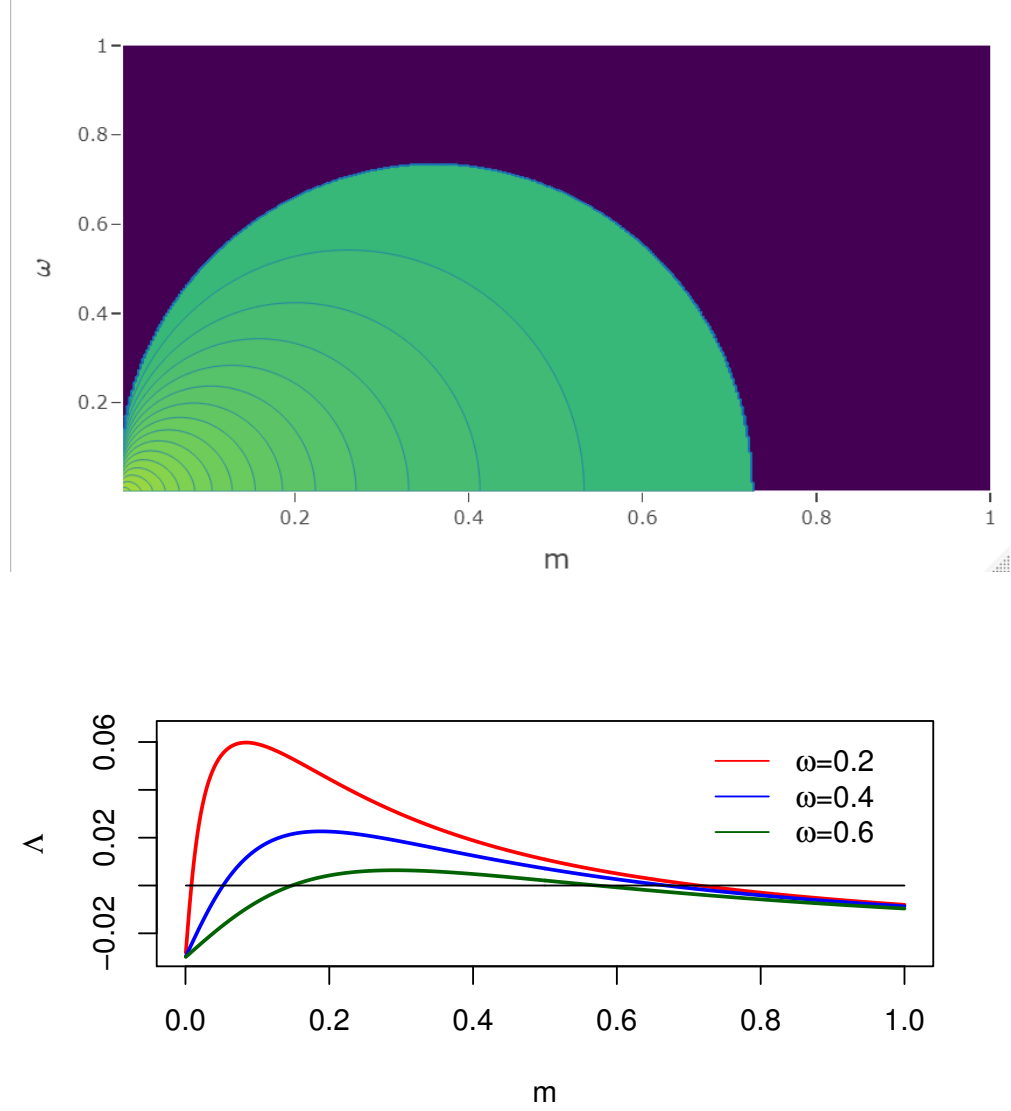


Figure 2: The Sink-Sink case. Top: Regions of growth (green) and decay (dark) for solutions of (1),(2) in the (m, ω) parameter plane. Also shown are level curves of the function $\Lambda(m, \omega)$. Bottom: Growth rate Λ of solutions of (1),(2) as a function of the dispersal rate m for three values of the frequency ω . Here $r_1(\omega t) = -0.03 + 0.3 \cos(\omega t)$, $r_2(\omega t) = r_1(\omega t - \pi) = -0.03 - 0.3 \cos(\omega t)$.

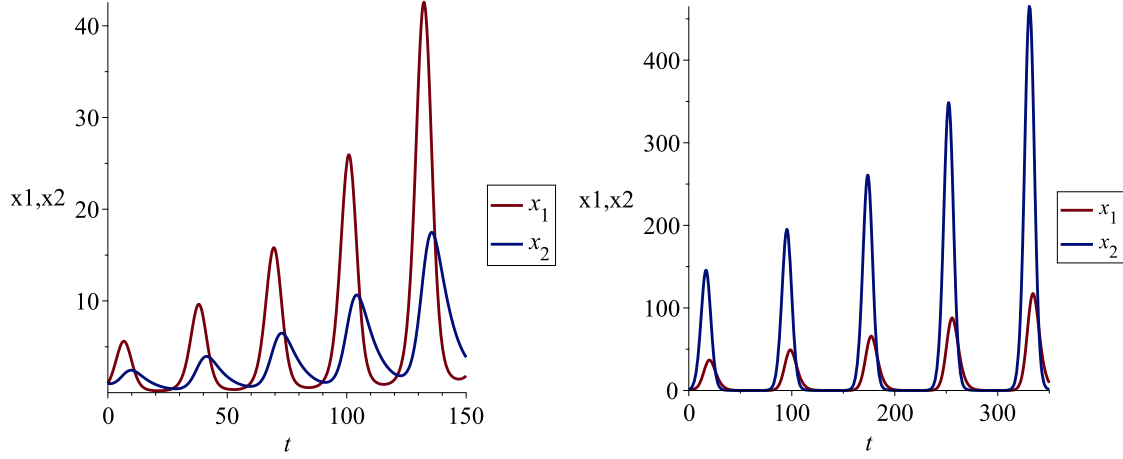


Figure 3: Left: Example of the DIG effect when growth rate in one of the patches is constant: $r_1(\omega t) = -0.05$, $r_2(\omega t) = -0.05 + 0.5 \cos(\omega t)$, $\omega = 0.2$, $m = 0.1$. Right: Example of DIG when the seasonal effect in the two patches is phase-synchronized: $r_1(\omega t) = -0.1 + 0.1 \cos(\omega t)$, $r_2(\omega t) = -0.1 + 0.6 \cos(\omega t)$, $\omega = 0.08$, $m = 0.05$.

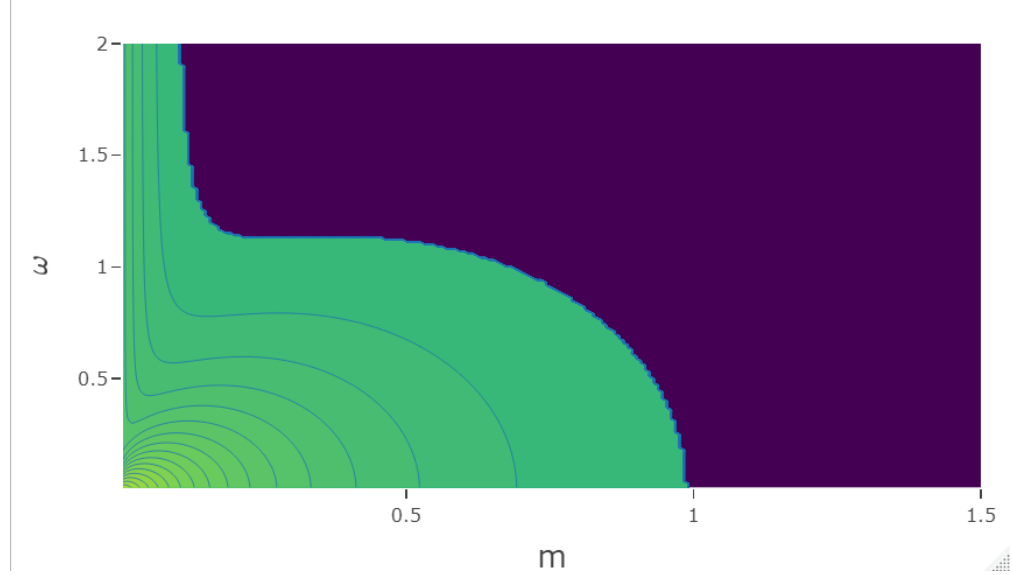


Figure 4: The Source-Sink case: Regions of growth (green) and decay (dark) for solutions of (1),(2) in the (m, ω) parameter plane. Also shown are level curves of the function $\Lambda(m, \omega)$. Here $r_1(\omega t) = -0.1 + 0.3 \cos(\omega t)$, $r_2(\omega t) = 0.05 - 0.3 \cos(\omega t)$.

exponents \bar{r}_1, \bar{r}_2 (see (3) above), so if these are both negative then, by continuity of the Floquet exponents with respect to parameters, these will also be negative for m sufficiently small, so that $\Lambda(m, \omega) < 0$.

(3) **Frequency of oscillations:** While Part (II),A of theorem 1 shows that, under the above-discussed conditions on the local growth rates and the dispersal, DIG will occur when $\omega > 0$ is *sufficiently small*, part (II),B of the theorem shows that for sufficiently high frequency ω , the DIG effect will *not* occur. Thus while time-variation is essential for DIG, the frequency of this variation cannot be too high.

2.4 The Source-Sink case

Although our main interest is in the DIG effect, which involves the the sink-sink case, we complement our analysis with a treatment of the source-sink case, using the same methods. Our results in this case are given by

Theorem 2 (Source-Sink case). *Assume $r_1(\theta)$, $r_2(\theta)$ are continuously differentiable 2π -periodic functions, with $\bar{r}_1\bar{r}_2 < 0$.*

(I) *If $\bar{r}_1 + \bar{r}_2 > 0$ then for any $m > 0, \omega > 0$ we have $\Lambda(m, \omega) > 0$ (growth).*

(II) *If $\bar{r}_1 + \bar{r}_2 < 0$ then:*

A. *(Low frequency)*

- *If $m \in (0, m^*)$ then for any $\omega > 0$ sufficiently small (depending on m), we have $\Lambda(m, \omega) > 0$ (growth).*
- *If $m > m^*$ then for any $\omega > 0$ sufficiently small (depending on m) we have $\Lambda(m, \omega) < 0$ (decay).*

B. *(High frequency)* Let

$$\hat{m} \doteq \left(\frac{1}{\bar{r}_1} + \frac{1}{\bar{r}_2} \right)^{-1}. \quad (8)$$

Then we have $0 < \hat{m} \leq m^*$ (where m^* is the solution of (7)), with strict inequality $\hat{m} < m^*$ unless $r_1(\theta) - r_2(\theta)$ is constant, and

- *If $m < \hat{m}$ then for ω sufficiently large (depending on m) we have $\Lambda(m, \omega) > 0$ (growth).*
- *If $m > \hat{m}$ then for ω sufficiently large (depending on m) we have $\Lambda(m, \omega) < 0$ (decay).*

The proof of part (I) of Theorem 2 will be given in section 3 (see Lemma 4). Parts (II) A,B of the theorem will be proved in sections 4,5, respectively.

Part (I) of the above theorem says that when the average of the two time-averaged growth rates is positive, growth always occurs. Part (II) says that growth may occur also when the average of the two growth rates is negative, and in contrast with the sink-sink case, here, if m is sufficiently small ($m < \hat{m}$), we have $\Lambda(m, \omega) > 0$ (growth) both when ω is sufficiently small *and* when ω is sufficiently large. This can be seen in the parameter-plane diagram in figure 4, obtained numerically, where it appears that when $m < \hat{m}$ growth occurs for all values of ω , while for $\hat{m} < m < m^*$ growth only occurs for ω sufficiently small.

Let us note that the condition $m < \hat{m}$ for growth in the high-frequency case is precisely the condition for growth in the case in which the local growth rates $r_1(\theta), r_2(\theta)$ are *constant*, with values \bar{r}_1, \bar{r}_2 (with $\bar{r}_1\bar{r}_2 < 0, \bar{r}_1 + \bar{r}_2 < 0$), that is the condition under which the dominant eigenvalue (5) of (4) is positive. Thus for high-frequency oscillations the time-periodic system behaves like the time averaged system. However, since, unless $r_1(\theta) - r_2(\theta)$ is constant, $\hat{m} < m^*$, part II-A of the theorem shows that, when the frequency is sufficiently small, the time periodic system also displays growth for parameter values for which the corresponding time-averaged system leads to decay.

3 Reduction to a one-dimensional differential equation

In this section we start proving the main results.

We first note that (1),(2) imply that

$$\begin{aligned} x_1 = 0, x_2 > 0 &\Rightarrow x'_1 > 0, \\ x_1 > 0, x_2 = 0 &\Rightarrow x'_2 > 0, \end{aligned}$$

which, by standard arguments, entail that any solution with non-negative initial conditions at $t = 0$ remains non-negative for all $t > 0$.

A key element enabling the analysis carried out in this work is the reduction of the problem to one of studying a single differential equation.

Lemma 1. *If (x_1, x_2) is a solution of (1),(2), then the function*

$$z(t) = \frac{x_2(t)}{x_1(t)}. \quad (9)$$

satisfies the differential equation

$$z' = (r_2(\omega t) - r_1(\omega t))z + m(1 - z^2). \quad (10)$$

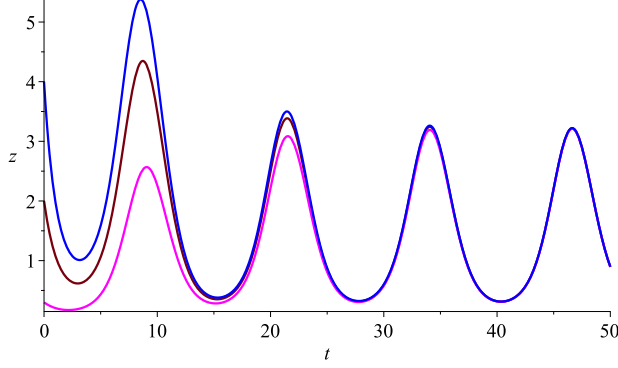


Figure 5: Illustration of the result of Lemma 2. All solutions of (10) approach a unique periodic solution. Here $m = 0.05$, $\omega = 0.5$, $r_1(\omega t) = -0.03 + 0.3 \cos(\omega t)$, $r_2(\omega t) = r_1(\omega t - \pi)$.

Proof. Dividing (1),(2) by x_1 we have

$$\frac{x'_1(t)}{x_1(t)} = r_1(\omega t) + mz(t) - m, \quad (11)$$

$$\frac{x'_2(t)}{x_1(t)} = r_2(\omega t)z(t) + m - mz(t), \quad (12)$$

from which it follows that

$$\begin{aligned} z'(t) &= \frac{x_1(t)x'_2(t) - x'_1(t)x_2(t)}{x_1(t)^2} = \frac{x'_2(t)}{x_1(t)} - \frac{x'_1(t)}{x_1(t)} \cdot z(t) \\ &= r_2(\omega t)z(t) + m - mz(t) - (r_1(\omega t) + mz(t) - m) \cdot z(t) = (r_2(\omega t) - r_1(\omega t))z(t) + m(1 - z(t)^2). \end{aligned}$$

□

Regarding the differential equation (10), we note that $z = 0$ implies $z' > 0$, so that any solution with positive initial condition remains positive for all $t > 0$. Moreover the following lemma shows that all solutions of (10) approach a unique periodic solution as $t \rightarrow \infty$ (see figure 5 for an illustration).

Lemma 2. *Assume $m > 0$. For each $\omega > 0$, there exists a unique $\frac{2\pi}{\omega}$ -periodic solution of (10), which we denote by $z_\omega(t)$, and this solution is globally stable, that is, all solutions $z(t)$ of (10) with $z(0) > 0$ satisfy*

$$\lim_{t \rightarrow \infty} [z(t) - z_\omega(t)] = 0. \quad (13)$$

Proof. We first transform (10) by making the change of variable $z(t) = e^{y(t)}$ (using the fact that $z(t)$ is positive), to obtain the equation

$$y' = (r_2(\omega t) - r_1(\omega t)) + m(e^{-y} - e^y). \quad (14)$$

We will show that (14) has a unique $\frac{2\pi}{\omega}$ -periodic solution $y_p(t)$ which is globally stable in the sense that, for any solution $y(t)$ of (14),

$$\lim_{t \rightarrow \infty} [y(t) - y_p(t)] = 0. \quad (15)$$

This will give the result of Lemma 2 for the equation (10). Denote by $y(t, y_0)$ the solution of (14) satisfying the initial condition $y(0) = y_0$. We define ψ to be the time- T ($T = \frac{2\pi}{\omega}$) Poincaré mapping corresponding to (14):

$$\psi(y_0) = y\left(\frac{2\pi}{\omega}, y_0\right).$$

To compute the derivative of this function we differentiate the equations

$$y_t(t, y_0) = (r_2(\omega t) - r_1(\omega t)) + m[e^{-y(t, y_0)} - e^{y(t, y_0)}], \quad y(0, y_0) = y_0$$

with respect to y_0 , obtaining

$$y_{y_0 t}(t, y_0) = -m[e^{-y(t, y_0)} + e^{y(t, y_0)}]y_{y_0}(t, y_0) \quad y_{y_0}(0, y_0) = 1,$$

leading to

$$y_{y_0}(t, y_0) = e^{-m \int_0^t (e^{-y(\tau, y_0)} + e^{y(\tau, y_0)}) d\tau},$$

so that

$$\psi'(y_0) = y_{y_0}(T, y_0) = e^{-m \int_0^T (e^{-y(\tau, y_0)} + e^{y(\tau, y_0)}) d\tau}$$

satisfies $0 < \psi'(y_0) < e^{-2mT} < 1$ for all y_0 . This implies that $\psi : \mathbb{R} \rightarrow \mathbb{R}$ is a contraction mapping, so that by Banach's contraction mapping principle it has a unique fixed point $y^* \in \mathbb{R}$, and, for all $y_0 \in \mathbb{R}$, the iterates of ψ satisfy

$$\lim_{k \rightarrow \infty} \psi^k(y_0) = y^*.$$

This, in turn, implies that the function $y_p(t) = y(t, y^*)$ is a periodic solution of (14), which is globally stable. \square

It should be noted that the periodic solution z_ω depends also on m , as well as on the periodic profiles $r_1(\theta), r_2(\theta)$ - however we suppress this dependence in our notation, since we will be studying the dependence of the periodic solution on ω .

We will now show that the periodic solution z_ω determines the growth rate Λ of x_1, x_2 .

Lemma 3. *Assume $m > 0, \omega > 0$. All solutions of (1),(2) with positive initial conditions satisfy*

$$\lambda[x_1] = \lambda[x_2] = \Lambda(m, \omega) = \bar{r}_1 + m \cdot \left(\frac{\omega}{2\pi} \int_0^{\frac{2\pi}{\omega}} z_\omega(\tau) d\tau - 1 \right). \quad (16)$$

Proof. By (11) and (13) we have

$$\begin{aligned} \lim_{t \rightarrow \infty} \frac{1}{t} \ln(x_1(t)) &= \lim_{t \rightarrow \infty} \frac{1}{t} \int_0^t \frac{x_1'(\tau)}{x_1(\tau)} d\tau \\ &= \lim_{t \rightarrow \infty} \frac{1}{t} \left[\int_0^t r_1(\omega\tau) d\tau + m \int_0^t (z(\tau) - 1) d\tau \right] = \bar{r}_1 + m \cdot \left(\frac{\omega}{2\pi} \int_0^{\frac{2\pi}{\omega}} z_\omega(\tau) d\tau - 1 \right). \end{aligned}$$

Note also that, by (9), and since (13) implies that any solution $z(t)$ of (10) is bounded on $[0, \infty)$, we have

$$\lim_{t \rightarrow \infty} \frac{1}{t} \ln(x_2(t)) = \lim_{t \rightarrow \infty} \frac{1}{t} [\ln(z(t)) + \ln(x_1(t))] = \lim_{t \rightarrow \infty} \frac{1}{t} \ln(x_1(t)).$$

\square

Note in particular that the growth rate does not depend on the initial conditions.

The parameter-plane plots in figures 2,4 were obtained by using Lemma 3: For each point in a grid in the plotted region, the periodic solution z_ω was found numerically, and the quantity $\Lambda(m, \omega)$ was computed. The green (growth) region is the set of points for which $\Lambda(m, \omega) > 0$.

There is an apparent asymmetry in the expression (16) in that only \bar{r}_1 appears explicitly, though of course z_ω depends on the functions $r_1(\theta), r_2(\theta)$. By exchanging the roles of $r_1(\theta)$ and $r_2(\theta)$, so that z_ω is replaced by $\frac{1}{z_\omega}$ we get the equivalent expression

$$\Lambda(m, \omega) = \bar{r}_2 + m \cdot \left(\frac{\omega}{2\pi} \int_0^{\frac{2\pi}{\omega}} \frac{1}{z_\omega(\tau)} d\tau - 1 \right). \quad (17)$$

and by averaging (16),(17) we obtain the symmetric expression:

$$\Lambda(m, \omega) = \frac{1}{2} (\bar{r}_1 + \bar{r}_2) + m \cdot \left(\frac{\omega}{2\pi} \int_0^{\frac{2\pi}{\omega}} \left(z_\omega(\tau) + \frac{1}{z_\omega(\tau)} \right) d\tau - 1 \right). \quad (18)$$

An advantage of this expression is that since the second term is evidently non-negative, and positive unless $z_\omega(t) \equiv 1$, we obtain the inequality

Lemma 4. *For any $m > 0, \omega > 0$, we have*

$$\Lambda(m, \omega) \geq \frac{1}{2} (\bar{r}_1 + \bar{r}_2),$$

with equality if and only if $r_1(\theta) \equiv r_2(\theta)$.

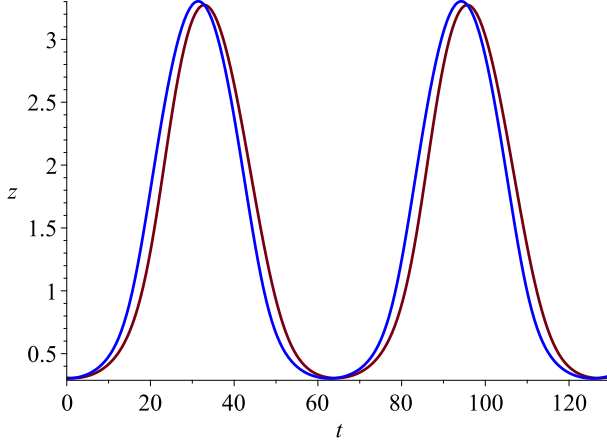


Figure 6: Illustration of the result of Lemma 6. The red curve is the periodic solution z_ω of (10), the blue curve is the function $Z(\omega t)$. Here $m = 0.2$, $\omega = 0.1$, $r_1(\omega t) = -0.03 + 0.3 \cos(\omega t)$, $r_2(\omega t) = r_1(\omega t - \pi)$.

In particular the above lemma implies part (I) of Theorem 2.

We conclude this section with an upper bound for $\Lambda(m, \omega)$, which in particular implies part (I) of Theorem 1.

Lemma 5. *For all $m > 0, \omega > 0$, we have*

$$\Lambda(m, \omega) \leq \chi.$$

Proof. We define $\eta(\theta) = \max(r_1(\theta), r_2(\theta))$. From (1),(2) we have

$$x'_1 \leq \eta(\omega t)x_1 + m(x_2 - x_1), \quad (19)$$

$$x'_2 \leq \eta(\omega t)x_2 + m(x_1 - x_2). \quad (20)$$

Adding (19),(20), and setting $x = x_1 + x_2$ we have

$$x'(t) \leq \eta(\omega t)x(t),$$

which implies

$$\begin{aligned} \Lambda(m, \omega) &= \lim_{t \rightarrow \infty} \frac{1}{t} \ln(x_1(t)) \leq \limsup_{t \rightarrow \infty} \frac{1}{t} \ln(x(t)) = \limsup_{t \rightarrow \infty} \frac{1}{t} \left[\ln(x(0)) + \int_0^t \frac{x'(\tau)}{x(\tau)} d\tau \right] \\ &\leq \limsup_{t \rightarrow \infty} \frac{1}{t} \int_0^t \eta(\omega \tau) d\tau = \frac{1}{2\pi} \int_0^{2\pi} \eta(\theta) d\theta = \chi. \end{aligned}$$

□

4 The low frequency limit

We will now obtain an explicit ‘adiabatic’ approximation for the periodic solution z_ω of (10) when the frequency ω is sufficiently small. In this ‘slowly varying’ case it makes intuitive sense that the solution $z(t)$ will track the equilibrium obtained by freezing the time-dependence in (10) - see Khalil and Grizzle [2002], Section 9.6 for a general discussion of results of this type for slowly varying systems. This intuition will be justified by Lemma 6 below.

For each θ we define $Z(\theta)$ as the unique positive solution of the quadratic equation obtained by setting the right-hand side of (10) (with $\theta = \omega t$) to 0:

$$(r_2(\theta) - r_1(\theta))Z(\theta) + m(1 - Z(\theta)^2) = 0, \quad (21)$$

or explicitly,

$$Z(\theta) = \frac{1}{2m} \left[r_2(\theta) - r_1(\theta) + \sqrt{(r_1(\theta) - r_2(\theta))^2 + 4m^2} \right]. \quad (22)$$

We claim that (see figure 6 for an illustration of the result):

Lemma 6. Assume $r_1(\theta), r_2(\theta)$ are continuously differentiable, and $m > 0$. Then we have

$$\max_t |z_\omega(t) - Z(\omega t)| = O(\omega), \quad \text{as } \omega \rightarrow 0.$$

Proof. We define

$$c = \frac{1}{m} \cdot \max_{\theta \in [0, 2\pi]} |Z'(\theta)|. \quad (23)$$

Henceforth we will assume that

$$0 < \omega < \frac{1}{c}, \quad (24)$$

and will show that we have

$$\max_t |z_\omega(t) - Z(\omega t)| < c\omega.$$

Since we know that z_ω is the *unique* positive periodic solution of (10) it suffices to prove that there exists a $\frac{2\pi}{\omega}$ -periodic solution $z(t)$ of (10) with

$$\max_t |z(t) - Z(\omega t)| < c\omega.$$

To do this, we re-write (10) by setting $z(t) = Z(\omega t) + d(t)$, obtaining

$$d' = (r_2(\omega t) - r_1(\omega t))(Z(\omega t) + d) + m(1 - (Z(\omega t) + d)^2) - \omega Z'(\omega t),$$

which, using (21) and (22) simplifies to

$$d' = f(t, d) = -md^2 - \sqrt{(r_1(\omega t) - r_2(\omega t))^2 + 4m^2} \cdot d - \omega Z'(\omega t). \quad (25)$$

We need to show that (25) has a $\frac{2\pi}{\omega}$ -periodic solution $d(t)$ satisfying

$$\max_t |d(t)| < c\omega. \quad (26)$$

Denote by $d(t, d_0)$ the solution of (25) satisfying the initial condition $d(0, d_0) = d_0$. We wish to show that

$$|d_0| \leq c\omega \Rightarrow |d(t, d_0)| < c\omega \quad \forall t > 0. \quad (27)$$

To obtain this property it is sufficient to have

$$f(t, c\omega) < 0, \quad f(t, -c\omega) > 0 \quad \forall t \geq 0. \quad (28)$$

Using the definition of $f(t, d)$ in (25) and the definition of c in (23), we have

$$\begin{aligned} f(t, c\omega) &= -mc^2\omega^2 - \sqrt{(r_1(\omega t) - r_2(\omega t))^2 + 4m^2} \cdot c\omega - \omega Z'(\omega t) < -2mc\omega - \omega Z'(\omega t) \\ &\leq -2m\omega c + \omega |Z'(\omega t)| \leq -2m\omega c + \omega mc = -mc\omega < 0, \end{aligned}$$

and, using (23) and (24),

$$\begin{aligned} f(t, -c\omega) &= -mc^2\omega^2 + \sqrt{(r_1(\omega t) - r_2(\omega t))^2 + 4m^2} \cdot c\omega - \omega Z'(\omega t) > -mc^2\omega^2 + 2m \cdot c\omega - \omega mc \\ &= mc\omega(1 - c\omega) > 0. \end{aligned}$$

We therefore have (28), and hence (27). This implies that the Poincaré map defined by

$$\rho(d_0) = d\left(\frac{2\pi}{\omega}, d_0\right)$$

satisfies $\rho([-c\omega, c\omega]) \subset (-c\omega, c\omega)$, which implies that it has a fixed point $d^* \in (-c\omega, c\omega)$: $\rho(d^*) = d^*$. Since (25) has $\frac{2\pi}{\omega}$ -periodic coefficients, it follows that $d(t) = d(d^*, t)$ is a $\frac{2\pi}{\omega}$ -periodic solution of (25), which, by (27) satisfies $|d(t)| < c\omega$ for all t . We have therefore proved the existence of a $\frac{2\pi}{\omega}$ -periodic solution of (25) satisfying (26), which concludes the proof of the lemma. \square

We now derive an explicit equation for the growth rate $\Lambda(m, \omega)$ in the limit $\omega \rightarrow 0$ (see figure 7 for an illustration of the contents of this result):

Lemma 7. Define

$$\Lambda_0(m) \doteq \frac{1}{2} \left[\bar{r}_1 + \bar{r}_2 + \frac{1}{2\pi} \int_0^{2\pi} \sqrt{(r_1(\theta) - r_2(\theta))^2 + 4m^2} d\theta \right] - m. \quad (29)$$

Then we have, for each $m > 0$:

$$\Lambda(m, \omega) = \Lambda_0(m) + O(\omega) \quad \text{as } \omega \rightarrow 0.$$

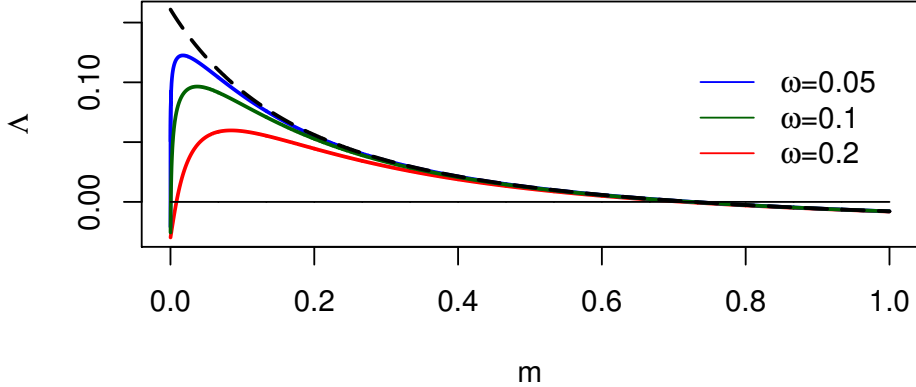


Figure 7: Illustration of the result of Lemma 4. Here $r_1(\omega t) = -0.03 + 0.3 \cos(\omega t)$, $r_2(\omega t) = r_1(\omega t - \pi)$. The curves $m \rightarrow \Lambda(m, \omega)$ are plotted for $\omega = 0.2, 0.1, 0.05$, and they can be seen to converge to the curve $\Lambda_0(m)$ (dashed line).

Proof. The uniform convergence in Lemma 6 implies

$$\begin{aligned} \left| \frac{\omega}{2\pi} \int_0^{\frac{2\pi}{\omega}} z_\omega(\tau) d\tau - \frac{1}{2\pi} \int_0^{2\pi} Z(\theta) d\theta \right| &= \left| \frac{\omega}{2\pi} \int_0^{\frac{2\pi}{\omega}} z_\omega(\tau) d\tau - \frac{\omega}{2\pi} \int_0^{\frac{2\pi}{\omega}} Z(\omega\tau) d\tau \right| \\ &\leq \frac{\omega}{2\pi} \int_0^{\frac{2\pi}{\omega}} |z_\omega(\tau) - Z(\omega\tau)| d\tau \leq \max_{0 \leq \tau \leq \frac{2\pi}{\omega}} |z_\omega(\tau) - Z(\omega\tau)| = O(\omega) \quad \text{as } \omega \rightarrow 0. \end{aligned}$$

Therefore from Lemma 3 we obtain

$$\begin{aligned} \Lambda(m, \omega) &= \bar{r}_1 + m \left(\frac{1}{2\pi} \int_0^{2\pi} Z(\theta) d\theta - 1 \right) + O(\omega) \\ &= \frac{1}{2} \left[\bar{r}_1 + \bar{r}_2 + \frac{1}{2\pi} \int_0^{2\pi} \sqrt{(r_1(\theta) - r_2(\theta))^2 + 4m^2} d\theta - 2m \right] + O(\omega) = \Lambda_0(m) + O(\omega). \end{aligned}$$

□

Lemma 7 implies that the sign of $\Lambda(m, \omega)$, is determined, for sufficiently small ω , by the sign of $\Lambda_0(m)$, given explicitly by (29).

The following lemma summarizes properties of the function $\Lambda_0(m)$, which will be used below:

Lemma 8. (i) The function $\Lambda_0(m)$ is decreasing on $[0, \infty)$.

(ii) $\Lambda_0(0) = \chi$, where χ is given by (6).

(iii) $\lim_{m \rightarrow \infty} \Lambda_0(m) = \frac{1}{2}(\bar{r}_1 + \bar{r}_2)$.

Proof. (i) We have

$$\Lambda'_0(m) = \frac{1}{2\pi} \int_0^{2\pi} \frac{2m}{\sqrt{[r_2(\theta) - r_1(\theta)]^2 + 4m^2}} d\theta - 1 < 0,$$

so that $\Lambda_0(m)$ is a decreasing function.

(ii) We have

$$\begin{aligned}\Lambda_0(0) &= \frac{1}{2} \left(\bar{r}_1 + \bar{r}_2 + \frac{1}{2\pi} \int_0^{2\pi} |r_2(\theta) - r_1(\theta)| d\theta \right) = \frac{1}{4\pi} \int_0^{2\pi} [r_1(\theta) + r_2(\theta) + |r_2(\theta) - r_1(\theta)|] d\theta \\ &= \frac{1}{2\pi} \int_0^{2\pi} \max(r_1(\theta), r_2(\theta)) d\theta = \chi.\end{aligned}$$

(iii) We have

$$\begin{aligned}\lim_{m \rightarrow +\infty} \Lambda_0(m) &= \frac{1}{2} \left(\bar{r}_1 + \bar{r}_2 + \lim_{m \rightarrow +\infty} \frac{1}{2\pi} \int_0^{2\pi} [\sqrt{[r_2(\theta) - r_1(\theta)]^2 + 4m^2} - 2m] d\theta \right) \\ &= \frac{1}{2} \left(\bar{r}_1 + \bar{r}_2 + \lim_{m \rightarrow +\infty} \frac{1}{2\pi} \int_0^{2\pi} \frac{[r_2(\theta) - r_1(\theta)]^2}{\sqrt{[r_2(\theta) - r_1(\theta)]^2 + 4m^2} + 2m} d\theta \right) = \frac{1}{2}(\bar{r}_1 + \bar{r}_2).\end{aligned}$$

□

We can now prove the parts of Theorems 1 and 2, pertaining to the low-frequency case.

Proof of Theorem 1, part (II), A: Assuming $\chi > 0$, Lemma 8 tells us that $\Lambda_0(m)$ is a decreasing function with $\Phi(0) > 0$ and since $\bar{r}_1 < 0, \bar{r}_2 < 0$, the limit of $\Lambda_0(m)$ as $m \rightarrow \infty$ is negative. We conclude that the equation $\Lambda_0(m) = 0$, equivalent to (7), has a unique solution m^* , and $\Lambda_0(m) > 0$ for $m \in (0, m^*)$, $\Lambda_0(m) < 0$ for $m > m^*$. Therefore if $m \in (0, m^*)$ then for sufficiently small ω we have $\Lambda(m, \omega) > 0$, and if $m > m^*$ then for sufficiently small ω we have $\Lambda(m, \omega) < 0$. □

Proof of Theorem 2, part (II), A: (i) If $\bar{r}_1 + \bar{r}_2 \geq 0$ then by Lemma 4 we have $\Lambda(m, \omega) > 0$.

(ii) If $\bar{r}_1 + \bar{r}_2 < 0$, then $\lim_{m \rightarrow \infty} \Lambda_0(m) < 0$ and, since

$$\Lambda_0(0) = \chi = \frac{1}{2\pi} \int_0^{2\pi} \max(r_1(\theta), r_2(\theta)) d\theta > \frac{1}{2\pi} \max \left(\int_0^{2\pi} r_1(\theta) d\theta, \int_0^{2\pi} r_2(\theta) d\theta \right) = \max(\bar{r}_1, \bar{r}_2),$$

which by the assumption $\bar{r}_1 \bar{r}_2 < 0$ implies that $\Lambda_0(0) > 0$. Therefore the equation $\Lambda_0(m) = 0$ has a unique solution m^* , and $\Lambda_0(m) > 0$ for $m \in (0, m^*)$, $\Lambda_0(m) < 0$ for $m > m^*$. Therefore if $m \in (0, m^*)$ then for sufficiently small ω we have $\Lambda(m, \omega) > 0$, and if $m > m^*$ then for sufficiently small ω we have $\Lambda(m, \omega) < 0$. □

5 The high frequency limit

We now study the behavior of the periodic solution z_ω of (10), and consequently of the growth rate $\Lambda(m, \omega)$, as $\omega \rightarrow \infty$. The following Lemma shows that when $\omega \rightarrow \infty$, z_ω converges uniformly to a constant function (see figure 8 for an illustration).

Lemma 9. *Fixing $m > 0$, the periodic solution z_ω of (10) satisfies*

$$\max_t \left| z_\omega(t) - \frac{1}{2m} \left(\bar{r}_2 - \bar{r}_1 + \sqrt{(\bar{r}_1 - \bar{r}_2)^2 + 4m^2} \right) \right| = O\left(\frac{1}{\omega}\right) \quad \text{as } \omega \rightarrow \infty, \quad (30)$$

and

$$\left| \frac{\omega}{2\pi} \int_0^{\frac{2\pi}{\omega}} z_\omega(t) dt - \frac{1}{2m} \left(\bar{r}_2 - \bar{r}_1 + \sqrt{(\bar{r}_1 - \bar{r}_2)^2 + 4m^2} \right) \right| = O\left(\frac{1}{\omega}\right) \quad \text{as } \omega \rightarrow \infty. \quad (31)$$

Proof. We set

$$z_\omega(t) = u_\omega(\omega t)$$

where $u_\omega(\theta)$ is 2π -periodic. From (10) we have that $u_\omega(\theta)$ satisfies

$$\omega u'_\omega(\theta) = (r_2(\theta) - r_1(\theta))u_\omega(\theta) + m(1 - u_\omega(\theta))^2. \quad (32)$$

We first obtain an apriori bound for the $u_\omega(t)$. If θ^* is a maximum point of u_ω , then, by (32), we have

$$(r_2(\theta^*) - r_1(\theta^*))u_\omega(\theta^*) + m(1 - u_\omega(\theta^*))^2 = 0,$$

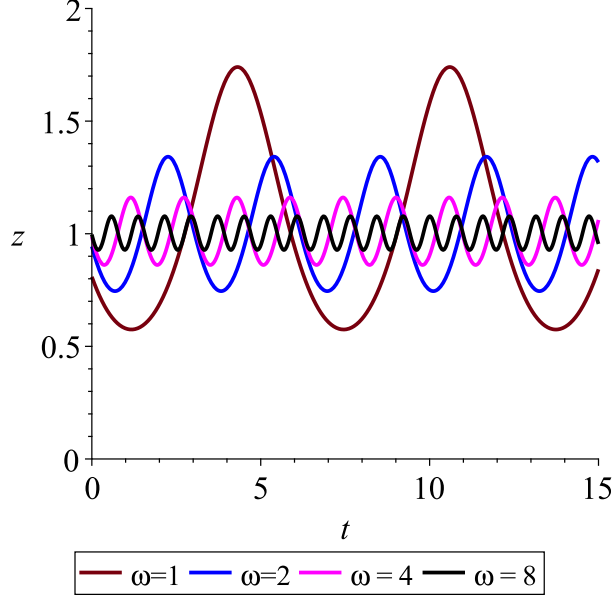


Figure 8: Illustration of the result of Lemma 9. The periodic solution z_ω is plotted for several values of ω . As ω , increases, the solution approaches a constant function. Here $m = 0.2$, $r_1(\omega t) = -0.03 + 0.3 \cos(\omega t)$, $r_2(\omega t) = r_1(\omega t - \pi)$.

so

$$u_\omega(\theta^*) = \frac{1}{2m} \left[(r_2(\theta^*) - r_1(\theta^*)) + \sqrt{(r_2(\theta^*) - r_1(\theta^*))^2 + 4m^2} \right].$$

We therefore conclude that

$$\max_\theta u_\omega(\theta) \leq C_1 = \frac{1}{2m} \max_\theta \left[(r_2(\theta) - r_1(\theta)) + \sqrt{(r_2(\theta) - r_1(\theta))^2 + 4m^2} \right]. \quad (33)$$

Therefore (32) implies

$$\omega |u'_\omega(\theta)| \leq C_1 |r_2(\theta) - r_1(\theta)| + m(1 + C_1^2) = C_2,$$

hence

$$\max_\theta |u'_\omega(\theta)| \leq C_2 \cdot \frac{1}{\omega},$$

implying

$$|u_\omega(\theta) - u_\omega(\phi)| \leq 2\pi \cdot C_2 \cdot \frac{1}{\omega}, \quad \forall \theta, \phi \in [0, 2\pi].$$

Therefore, defining

$$M_\omega = \frac{\omega}{2\pi} \int_0^{\frac{2\pi}{\omega}} z_\omega(\omega t) dt = \frac{1}{2\pi} \int_0^{2\pi} u_\omega(\theta) d\theta,$$

we have, for all $\theta \in [0, 2\pi]$,

$$|u_\omega(\theta) - M_\omega| = \left| \frac{1}{2\pi} \int_0^{2\pi} [u_\omega(\theta) - u_\omega(\phi)] d\phi \right| \leq \frac{1}{2\pi} \int_0^{2\pi} |u_\omega(\theta) - u_\omega(\phi)| d\phi \leq 2\pi \cdot C_2 \cdot \frac{1}{\omega}. \quad (34)$$

Integrating both sides of (32) over $[0, 2\pi]$ we obtain

$$\frac{1}{2\pi} \int_0^{2\pi} (r_2(\theta) - r_1(\theta)) u_\omega(\theta) d\theta + m - m \cdot \frac{1}{2\pi} \int_0^{2\pi} u_\omega(\theta)^2 d\theta = 0,$$

which, together with (34), implies, as $\omega \rightarrow \infty$,

$$\frac{1}{2\pi} \int_0^{2\pi} (r_2(\theta) - r_1(\theta)) M_\omega d\theta + m - m \cdot \frac{1}{2\pi} \int_0^{2\pi} M_\omega^2 d\theta = O\left(\frac{1}{\omega}\right),$$

that is

$$M_\omega \cdot (\bar{r}_2 - \bar{r}_1) + m - m \cdot M_\omega^2 = O\left(\frac{1}{\omega}\right),$$

or

$$\begin{aligned} M_\omega &= \frac{1}{2m} \left[\bar{r}_2 - \bar{r}_1 + \sqrt{(\bar{r}_1 - \bar{r}_2)^2 + 4m \left(m + O\left(\frac{1}{\omega}\right) \right)} \right] \\ &= \frac{1}{2m} \left(\bar{r}_2 - \bar{r}_1 + \sqrt{(\bar{r}_1 - \bar{r}_2)^2 + 4m^2} \right) + O\left(\frac{1}{\omega}\right). \end{aligned}$$

Therefore we have (31), and together with (34), we have (30). \square

Using Lemma 3 and (31) we have, as $\omega \rightarrow \infty$,

$$\Lambda(m, \omega) = \bar{r}_1 + m \cdot \left(\frac{\omega}{2\pi} \int_0^{\frac{2\pi}{\omega}} z_\omega(\tau) d\tau - 1 \right) = \frac{1}{2} \left(\bar{r}_1 + \bar{r}_2 + \sqrt{(\bar{r}_1 - \bar{r}_2)^2 + 4m^2} \right) - m + O\left(\frac{1}{\omega}\right),$$

so we have proved

Lemma 10. *Define*

$$\Lambda_\infty(m) = \frac{1}{2} \left[\bar{r}_1 + \bar{r}_2 + \sqrt{(\bar{r}_1 - \bar{r}_2)^2 + 4m^2} \right] - m. \quad (35)$$

Then we have, for all $m > 0$,

$$\Lambda(m, \omega) = \Lambda_\infty(m) + O\left(\frac{1}{\omega}\right), \quad \text{as } \omega \rightarrow \infty.$$

We can now give the

Proof of Theorem 1, part (II), B: When $\bar{r}_1 + \bar{r}_2 < 0$ we have

$$\Lambda_\infty(m) < 0 \Leftrightarrow \sqrt{(\bar{r}_1 - \bar{r}_2)^2 + 4m^2} < 2m - \bar{r}_1 - \bar{r}_2 \Leftrightarrow m(\bar{r}_1 + \bar{r}_2) < \bar{r}_1 \bar{r}_2, \quad (36)$$

and since here we are assuming $\bar{r}_1 < 0$ and $\bar{r}_2 < 0$, the last inequality holds, so we have $\Lambda_\infty(m) < 0$ for all m , hence, by Lemma 10 for any m and for ω sufficiently large we have $\Lambda(m, \omega) < 0$. \square

Proof of Theorem 2, part (II), B: Assuming $\bar{r}_1 + \bar{r}_2 < 0$, we have (36), implying that $\Lambda_\infty(m) < 0$ if $m < \hat{m}$, and $\Lambda_\infty(m) > 0$ if $m > \hat{m}$, where \hat{m} is defined by (8). This implies that if $m < \hat{m}$ then $\Lambda(m, \omega) > 0$ for ω sufficiently large, and if $m > \hat{m}$ then $\Lambda(m, \omega) < 0$ for ω sufficiently large.

It remains only to prove the claim that $\hat{m} < m^*$. To see this, we define

$$f(\theta) = r_2(\theta) - r_1(\theta), \quad \varphi(y) = \sqrt{y^2 + 4m^2},$$

and note that the function φ is convex, so Jensen's inequality implies

$$\varphi\left(\frac{1}{2\pi} \int_0^{2\pi} f(\theta) d\theta\right) \leq \frac{1}{2\pi} \int_0^{2\pi} \varphi(f(\theta)) d\theta,$$

with equality iff $f(\theta)$ is constant, that is

$$\sqrt{(\bar{r}_2 - \bar{r}_1)^2 + 4m^2} \leq \frac{1}{2\pi} \int_0^{2\pi} \sqrt{|r_2(\theta) - r_1(\theta)|^2 + 4m^2} d\theta,$$

which, by (29),(35) implies

$$\Lambda_\infty(m) \leq \Lambda_0(m).$$

Therefore

$$\Lambda_0(m^*) = 0 = \Lambda_\infty(\hat{m}) \leq \Lambda_0(\hat{m}),$$

which, since Λ_0 is a decreasing function, implies $\hat{m} \leq m^*$. Moreover equality can only occur if $r_1(\theta) - r_2(\theta)$ is constant. \square

6 Discussion

The DIG effect is an interesting example of an emergent dynamical phenomena which arises from the combination of several elementary mechanisms, and which cannot occur if any of the mechanisms are excluded. The mechanisms here are: (i) Temporal heterogeneity: population growth rate of at least one patch varies in time. (ii) Spatial heterogeneity: the population growth rate profiles in the two patches are not identical, (iii) Dispersal among the patches. Given these mechanisms we have seen that the populations can persist and grow despite the fact that each of the patches is a sink. In the absence of any one of these three mechanisms, population growth could not occur when both patches are sinks.

We have proved that DIG is a *robust* phenomenon, as it occurs *regardless* of the specific choice of the periodic local growth-rate profiles $r_1(\theta), r_2(\theta)$, as long as the condition $\chi > 0$ holds (with χ given by (6)), for a range of values of the frequency ω of the oscillations in growth rates and of the dispersal rate m . However we have seen that in order for DIG to occur, it is necessary that the frequency ω not be too large, and that the dispersal rate m is neither too small *nor* too large.

We now return to the numerical results presented in figure 2, as discussed in section 2.2, and point out some features observed in this figure, and in analogous figures we have plotted for other periodic profiles $r_1(\theta), r_2(\theta)$, which we have not so far been able to rigorously prove. Below we assume $\bar{r}_1 < 0, \bar{r}_2 < 0$, and $\chi > 0$, so that, by Theorem 1 the set of parameters for which DIG occurs is nonempty.

As we see in figure 2, for $m \in (0, m^*)$ (where the m^* was explicitly given in Theorem 1), there exists a value $\omega_{crit}(m)$ so that DIG occurs for $\omega < \omega_{crit}(m)$ and does not occur for $\omega > \omega_{crit}(m)$. This is consistent with the results of Theorem 1 which say that, when $m \in (0, m^*)$, DIG occurs for ω sufficiently small, and does not occur for ω sufficiently large. However, our theorem does not imply the existence of a *unique* transition point $\omega_{crit}(m)$ - it does not exclude the possibility that several such transitions from growth to decay and back occur as ω increases. If it could be proved that the function $\Lambda(m, \omega)$ is monotone decreasing in ω , for fixed m , then it would follow from Theorem 1 that there is a unique transition value $\omega_{crit}(m)$, given, for each $m \in (0, m^*)$, by the solution of the equation $\Lambda(m, \omega) = 0$. We therefore formulate

Conjecture 1. *The function $\Lambda(m, \omega)$ satisfies $\Lambda'_\omega(m, \omega) < 0$ for all $m > 0, \omega > 0$.*

Since $\Lambda(m, \omega)$ is given an explicit way by (16) (or (18)), it follows that proving the above conjecture requires studying the dependence of the periodic solution z_ω on the parameter ω . Assuming the validity of Conjecture 1, it also follows, using the implicit function theorem, that the quantity $\omega_{crit}(m)$ is a smooth function of m . We also note that if the conjecture is valid then it follows that when $m > m^*$ DIG does *not* occur for *any* $\omega > 0$, since we know from Theorem 1 that $\Lambda(m, \omega) < 0$ for ω small, so the monotonicity would imply the same for all ω .

Our results imply some key properties of the curve $\omega = \omega_{crit}(m)$ - the upper boundary of the green region in figure 2. The fact that $\omega_{crit}(m^*) = 0$ follows from Theorem 1, since we know that for $m > m^*$ we have $\Lambda(m, \omega) < 0$ for ω small. The fact that $\omega_{crit}(0) = 0$ is also easy to understand, since if we have $\omega_{crit}(0) > 0$ then, for fixed $\omega \in (0, \omega_{crit}(0))$, DIG would occur for arbitrarily small m , which would contradict the continuity of Floquet exponents as functions of the parameters, since we know that when $m = 0$ the Floquet exponents are \bar{r}_1, \bar{r}_2 , which we assume are negative.

The shape of the curve $\omega = \omega_{crit}(m)$, as observed in figure 2, leads us to the following

Conjecture 2. *The function $\omega_{crit} : (0, m^*) \rightarrow (0, \infty)$ is concave.*

The behavior of the curve $\omega = \omega_{crit}(m)$ in the vicinity of $m = 0$ is also not well-understood. From the numerical results it seems evident that this curve is tangent to the ω -axis at the origin, but we have not been able to show this analytically, and therefore formulate

Conjecture 3. *The function ω_{crit} satisfies $\lim_{m \rightarrow 0} \omega'_{crit}(m) = +\infty$.*

We note that this conjecture, if true, means that for small ω very weak dispersal is sufficient to cause DIG. Proving this conjecture requires studying the function $\Lambda(m, \omega)$ when m and ω are simultaneously small, that is approximating the periodic solution z_ω in this regime - which is not captured by our results in section 4, which assumed ω small and $m > 0$ fixed. It seems that some additional analytical ideas are needed to treat this problem.

Another important direction for further investigation is to obtain analytical results on the occurrence of DIG in more general deterministic models with time-periodic environmental variation. Extending from two to more patches presents additional technical difficulties, though some of the ideas used here can be generalized. When many patches are involved there are various possibilities for the spatial structure defining the dispersal, and it would be interesting to better understand the effect of this structure on the occurrence and strength of DIG. Such improved understanding

would also enable to better assess the extent and the circumstances under which the DIG effect is relevant to explaining population persistence and growth in real-world ecosystems.

References

K. C. Abbott. A dispersal-induced paradox: synchrony and stability in stochastic metapopulations. *Ecology letters*, 14(11):1158–1169, 2011.

M. Baguette, T. G. Benton, and J. M. Bullock. *Dispersal ecology and evolution*. Oxford University Press, 2012.

V. Bansaye and A. Lambert. New approaches to source–sink metapopulations decoupling demography and dispersal. *Theoretical population biology*, 88:31–46, 2013.

J. Bascompte, H. Possingham, and J. Roughgarden. Patchy populations in stochastic environments: critical number of patches for persistence. *The American Naturalist*, 159(2):128–137, 2002.

K. H. Cheong, J. M. Koh, and M. C. Jones. Paradoxical survival: Examining the parrondo effect across biology. *BioEssays*, 41(6):1900027, 2019.

R. Cousens, C. Dytham, and R. Law. *Dispersal in plants: a population perspective*. Oxford University Press, 2008.

P. C. Dias. Sources and sinks in population biology. *Trends in Ecology & Evolution*, 11(8):326–330, 1996.

S. N. Evans, P. L. Ralph, S. J. Schreiber, and A. Sen. Stochastic population growth in spatially heterogeneous environments. *Journal of mathematical biology*, 66(3):423–476, 2013.

J. K. Hale. *Ordinary Differential Equations, reprint edn*. Dover Publications, 2009.

I. A. Hanski and O. E. Gaggiotti. *Ecology, genetics and evolution of metapopulations*. Academic Press, 2004.

P. J. Hudson and I. M. Cattadori. The Moran effect: a cause of population synchrony. *Trends in ecology & evolution*, 14(1):1–2, 1999.

V. A. Jansen and J. Yoshimura. Populations can persist in an environment consisting of sink habitats only. *Proceedings of the National Academy of Sciences*, 95(7):3696–3698, 1998.

T. J. Kawauchi. Ecological and evolutionary consequences of source-sink population dynamics. *Ecology, genetics and evolution of metapopulations*, pages 387–414, 2004.

H. K. Khalil and J. W. Grizzle. *Nonlinear Systems*, volume 3. Prentice hall Upper Saddle River, NJ, 2002.

C. A. Klausmeier. Floquet theory: a useful tool for understanding nonequilibrium dynamics. *Theoretical Ecology*, 1(3):153–161, 2008.

N. Kortessis, M. W. Simon, M. Barfield, G. E. Glass, B. H. Singer, and R. D. Holt. The interplay of movement and spatiotemporal variation in transmission degrades pandemic control. *Proceedings of the National Academy of Sciences*, 117(48):30104–30106, 2020.

M. A. Lewis, S. V. Petrovskii, and J. R. Potts. *The mathematics behind biological invasions*, volume 44. Springer, 2016.

D. P. Matthews and A. Gonzalez. The inflationary effects of environmental fluctuations ensure the persistence of sink metapopulations. *Ecology*, 88(11):2848–2856, 2007.

J. Metz, T. De Jong, and P. Klinkhamer. What are the advantages of dispersing; a paper by Kuno explained and extended. *Oecologia*, 57(1-2):166–169, 1983.

S. Morita and J. Yoshimura. Analytical solution of metapopulation dynamics in a stochastic environment. *Physical Review E*, 86(4):045102, 2012.

H. R. Pulliam. Sources, sinks, and population regulation. *The American Naturalist*, 132(5):652–661, 1988.

M. Roy, R. D. Holt, and M. Barfield. Temporal autocorrelation can enhance the persistence and abundance of metapopulations comprised of coupled sinks. *The American Naturalist*, 166(2):246–261, 2005.

S. J. Schreiber. Interactive effects of temporal correlations, spatial heterogeneity and dispersal on population persistence. *Proceedings of the Royal Society B: Biological Sciences*, 277(1689):1907–1914, 2010.

E. R. White and A. Hastings. Seasonality in ecology: Progress and prospects in theory. *Ecological Complexity*, 44:100867, 2020.

P. D. Williams and A. Hastings. Paradoxical persistence through mixed-system dynamics: towards a unified perspective of reversal behaviours in evolutionary ecology. *Proceedings of the Royal Society B: Biological Sciences*, 278(1710):1281–1290, 2011.